Detection Limits and Planet Occurrence Rate in the CARMENES Sample

Author. Juan Carlos Muñoz Sánchez. Tutor: Juan Carlos Morales. Tutor UB: Carme Jordi.

Abstract. – The CARMENES survey is monitoring more than 300 M-dwarf stars looking for exoplanets. Besides planet discoveries, the data it produces can also be used to estimate the statistics of planets around late-type stars. In this work, we aim at estimating the detection limits of the CARMENES survey, and the occurrence rate of Jupiter- and Neptune-like planets around M-dwarf stars. For this purpose, we use a sample with 324 stars for which values for the radial velocity as a function of time have been measured. We remove the signals produced by planets or intrinsic stellar variability to analyse the instrumental noise. In this noise we look for the minimum planetary mass that could be discovered, obtaining a lower detection limit. With this result we estimate the occurrence rate of M-dwarf planets at different minimum mass and orbital period ranges. For Jupiter- and Neptune-like planets we obtained an occurrence rate of $\sim 1\%$.

Keywords: stars: late-type – planetary systems, technique: radial velocities, instrumentation: spectrographs

1.- INTRODUCTION

We could say it was in 1989 when the flame of the exoplanet research field was kindled after the first detection of a planet outside the solar system. Although Latham et al. (1989) thought, at first, that the companion to HD114762 was a brown dwarf, Cochran et al. (1991) confirmed, using high-precision measurements of the velocity of the star along the line of sight (hereafter radial velocity), that it was an exoplanet of about 10 M_J (Jupiter masses). It was, however, in the early 90's when Wolszczan and Frail (1992) performed the first convincing detection of planetary mass bodies beyond the Solar System discovering a system with two planets orbiting the pulsar PSE1257+12 with masses around 2.8 and 3.4 $M_\oplus$ (Earth masses). Few years later, Mayor and Queloz (1995) announced the first unambiguous detection of a planet orbiting a main sequence star by means of radial velocity measurements. Since then, thanks to the instrumental advances that have been made, 4164 exoplanets have been discovered.

Figure 1 illustrates the different techniques that can be used to detect exoplanets (Perryman, 2018). Figures beside each technique indicate the number of detected exoplanets by 2018, showing that the most efficient methods are astrometry, microlensing, direct imaging, transit detection and radial velocity measurements using high-resolution spectroscopy. Let us briefly summarize the main characteristics of these five main methods:

Astrometry: the presence of a planet is revealed by the movements of the host star around the centre of mass of the system, which is observed as a change of the position of the star on the sky. It is a particularly sensitive technique to detect long periods (P > 1 yr) planets in wide orbits. It also applies to very hot stars and fast rotating stars, whose planets can be difficult to detect using spectroscopic techniques. The Gaia mission is expected to make a significant contribution to the knowledge of exoplanet systems (Ranalli et al., 2018).
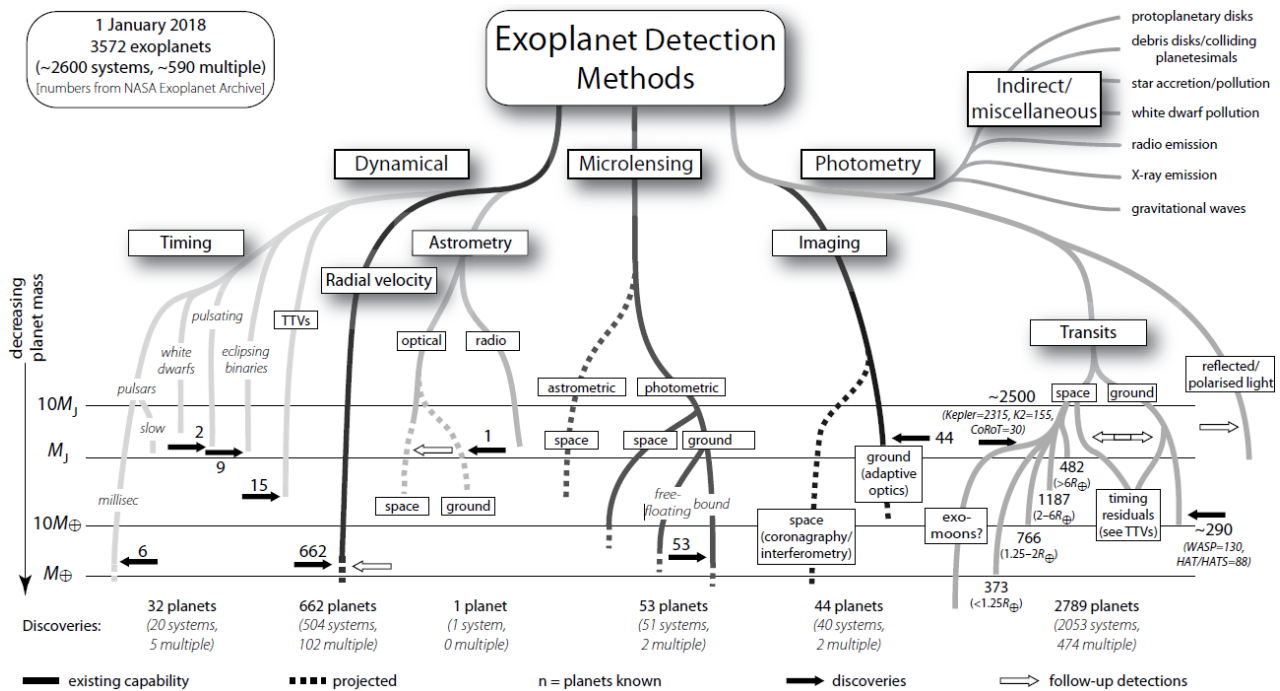
Figure 1.- Diagram showing the different methods to discover exoplanets, and they number of planets they have detected. Numbers come from the NASA Exoplanet Archive at 2018 January first. As can be seen, at this moment several methods had been developed. Figure from The Exoplanet Handbook by Michael Perryman (Perryman, 2018).

Microlensing: this technique takes advantage of the gravitational lens effect that the planetary system causes on a distant star that acts as a point source. Because the images generally appear close to the Einstein ring, microlensing is most sensitive to planets with projected separations equal to the physical size of the Einstein ring in the lens plane (Fischer et al., 2014). Many of the planets discovered by microlensing have large mass ratios with respect to the host star and correspond to Jovian planets. 2.1% of the exoplanet discoveries made to date have been through the microlensing technique, positioning this method as the third in number of discovered planets.

Direct Imaging: with this technique some planets can be observed when removing the powerful glare of their host star. Although currently only 49 planets have been discovered using this technique there is a high expectation it will eventually be a key tool for finding and characterizing exoplanets because of rapid improvement of instruments. The main advantage is that light from the planet is directly observed. Future direct-imaging instruments might be able to take images of exoplanets that would allow us to identify atmospheric patterns, oceans, and landmasses (NASA Exoplanet Archive, 2020).

Transits: if correct alignment occurs, planets can totally or partially block the light of a star causing a depression in its light curve, i.e. a transit. The study of this transit allows to estimate parameters of the planet such as the radius. If we estimate the mass trough radial velocity techniques, we can easily obtain the density of the planet. The transit technique also allows obtaining additional information such as its composition or atmospheric structure. This type of technique is especially used in M-type stars since, due to their size,

Earth-sized planets can be more easily distinguished than when orbiting solar-type stars. From the ground, two instruments have been responsible for most of the transiting planets discovered: HAT (Hungarian-made Automated Telescope; Bakos et al., 2004) and WASP (Wide Angle Search for Planets; Pollacco et al., 2006). The MEarth Project (Berta et al., 2012) is also an example of such surveys, but particularly focused on looking for transiting exoplanets around nearby M-dwarf stars using robotic telescopes. However, it was with the Kepler satellite (2009-2013; Borucki, 2011) when the number of detections using this technique rapidly increased. Following it success, the TESS satellite (Transiting Exoplanet Survey Satellite; Ricker et al., 2015) is surveying the whole sky and has already provided more than 2000 planet candidates which are being confirmed by other techniques. All in all, currently 3169 planets have been discovered by looking for transits, which corresponds to 76.1% of the total detections.

Radial velocity measurements: this technique is based on the measurement of the orbit of the star around the barycentre of the system due to the presence of one or more planets. The Doppler effect allows to measure the velocity of the stars along the line of sight, known as radial velocity, from high resolution spectroscopic observations. As previously mentioned, this was one of the first techniques used to search for exoplanets and continues to be one of the most productive. Furthermore, this technique is used to confirm planets detected by transits by estimating their mass. Currently the precision of this technique allows detecting changes in the radial velocity of the stars of about 1 m/s. Several instruments, such as HARPS (High Accuracy Radial Velocity Planet Searcher; Mayor et al., 2003) and CARMENES (Calar Alto high-Resolution search for M dwarfs with Exoearths with Near-infrared and optical Echelle Spectrographs; Quirrenbach et al., 2014) reach this level of precision and are used to discover and characterize exoplanets. For this work, we use the data from the CARMENES instrument consisting of two separate echelle spectrographs covering the wavelength range from 0.55 to 1.7 μm (optimal range for the study of M-type stars). The 19.3% of the planets known up to now have been discovered using radial velocity measurements, in total 804 planets.

The rapid growth of the exoplanet research field, and the increasing number of discovered exoplanets, has also triggered the study of the processes of planet formation and evolution with the goal of explaining the diversity of systems. To date, the generally accepted model to explain planet formation is the core accretion model (Lissauer, 1993; Pollack et al., 1996; Safronov, 1972), including mechanism such as migration or pebble accretion to predict some type of planets (Ormel and Klahr, 2010; Lambrechts and Johansen, 2012). In the pebble accretion mechanism protoplanets accrete smaller objects from the disk (cm- to m-sized) called pebbles instead of km-sized planetesimals. In this scenario accretion rate increases approximately one order of magnitude when comparing with the classical planetesimal core accretion model (Lambrechts et al., 2014; Brouwers et al., 2018) as pebbles are more susceptible to gas drag. The largest planetesimals can then continue growing by accreting other planetesimals as well as pebbles left over from planetesimal formation (Johansen and Lambrechts, 2017). If these cores reach sufficient mass (surface gravity) to retain the H+He gas while the disk is still gas rich, then a giant gas planet can be formed. This model is able to predict almost all the different planets known until now, and therefore it is widely accepted in the exoplanet community.

However, the detection of the planet GJ3512b (Morales, 2019) challenges this formation model, even forcing its parameters, and it is necessary to take into account new scenarios. GJ3512b, discovered thanks to CARMENES observations, is a Jupiter-like exoplanet with a minimum mass of $m \sin i = 0.463^{+0.022}_{-0.023}\,\mathrm{M_J}$ orbiting an M-type star, GJ5312, with mass $M_* = 0.123 \pm 0.009\,\mathrm{M_\odot}$. The orbital period is $P = 203.59^{+0.14}_{-0.14}$ days and its semi-major axis $a = 0.3380^{+0.008}_{-0.008}$ AU. As illustrated in Figure 2, which depicts the evolution of planetesimals at different ages in the pebble accretion model for a solar-type star and GJ 3512, according to this model a planet of these characteristics cannot be formed around such a star. However, there is another mechanism capable of explaining the formation of this planet. This mechanism is known as gravitational disk instability (Boss, 1997; Cameron, 1978; Kuiper, 1951). It entails the formation of planets from the breakup of a protoplanetary disk due to gravitational instability forming an initial overdensity, which causes self-gravitating clumps of gas. If the gravitational potential energy of these clumps is sufficient to prevent rupture by pressure and differential rotation, they may eventually collapse forming a planet. It is a fast process and results in a planet whose composition is directly related to the local composition of the disk. This method usually predicts planets that are generally too massive when comparing with observations. However, the discovery of GJ3512b indicates that gravitational instability may also play a role in the formation of giant planets around low-mass stars. Considering these results, we wonder how common this configuration is, that is, what is the expected occurrence rate of planets of these characteristics orbiting M-type stars. This will allow us to discuss the importance of both models and their possible coexistence, as well as to optimize the strategy and increase the efforts in the search for similar planets.

To do this, we use the data obtained by the CARMENES spectrograph for a set of 324 M-type stars. Following the techniques explained in section 3 we obtain the planet detection limits of each star and infer the expected occurrence rate for Jupiter- and Neptune-like planets around late-type stars.

Before going on to explain the experimental procedure, it is worth to clarify first the different classifications used when referring to planets. Both the definition of planets and their classification have been the subject of constant debate. In 2003 the International Astronomical Union (IAU) established a first difference between planets, brown dwarfs, and brown sub-dwarfs. Between the two former cases, the upper limit of $13\mathrm{M_J}$ was established for planets (mass limit to start the combustion of deuterium; Spiegel, 2011). The brown sub-dwarfs were defined as "free-floating objects in young star clusters with masses below the limiting mass for thermonuclear fusion of deuterium". However, this definition based on the combustion of deuterium did not have a solid justification and led to confusion, so in 2006 the convention suggested by Soter (2006) was adopted. Using this convention: "A planet is an end product of disk accretion around a primary star or a substar". With this new definition, the upper limit mass to be considered a planet would be around 25–30 $\mathrm{M_J}$. In fact, Schneider et al. (2011) assigned a mass of $25\mathrm{M_J}$ as the upper limit for including objects in the Exoplanet Encyclopaedia. There are different classifications within the category of planets dividing them, for example, according to sizes, temperatures or masses. In the mass classification, which is the most extensive, Stevens and Gaudi (2013) establish different categories: sub-Earths, Earths, super-Earths, Neptunes, Jupiters, super-Jupiters, brown dwarfs and stellar companions as can be seen in Figure 3. Therefore, when we talk about Jupiter-type planets, we are referring to masses between approximately 100 and 1000 $\mathrm{M_\oplus}$.

Time = 0.125 million years   Time = 0.250 million years

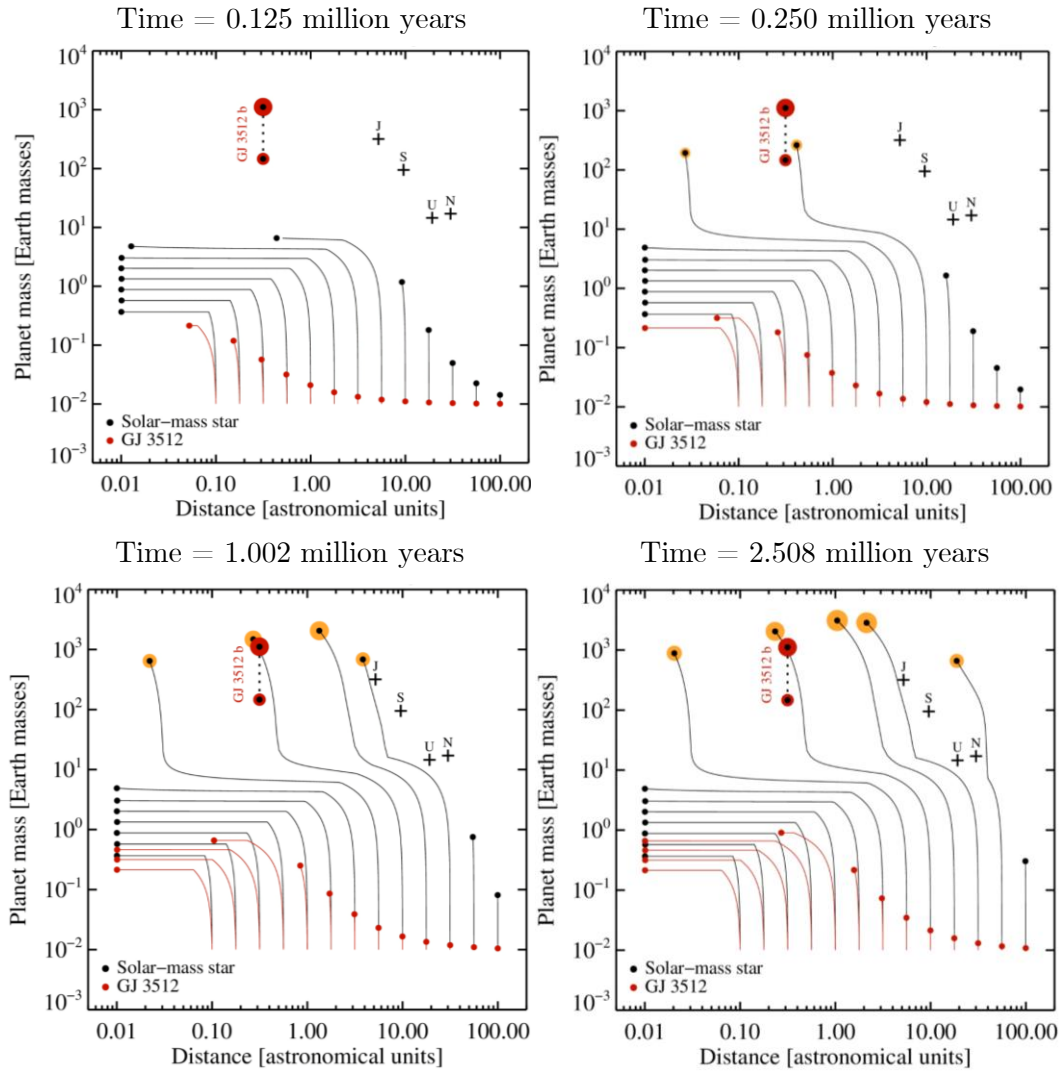Time = 1.002 million years   Time = 2.508 million years

Figure 2.- Four frames of a simulation showing that pebble accretion scenario can explain the formation of planets such as Jupiter and Saturn around Sun-type stars (black lines) but fails to explain the formation of GJ3512b around a red M dwarf (red lines). The time since the onset of planet formation is indicated at the top of each panel. Cross symbols correspond to mass and orbital distance of Jupiter (J), Saturn (S), Uranus (U), and Neptune (N) in the Solar System. Figure from A. Johansen at Lund Observatory (IEEC press release, 2019).
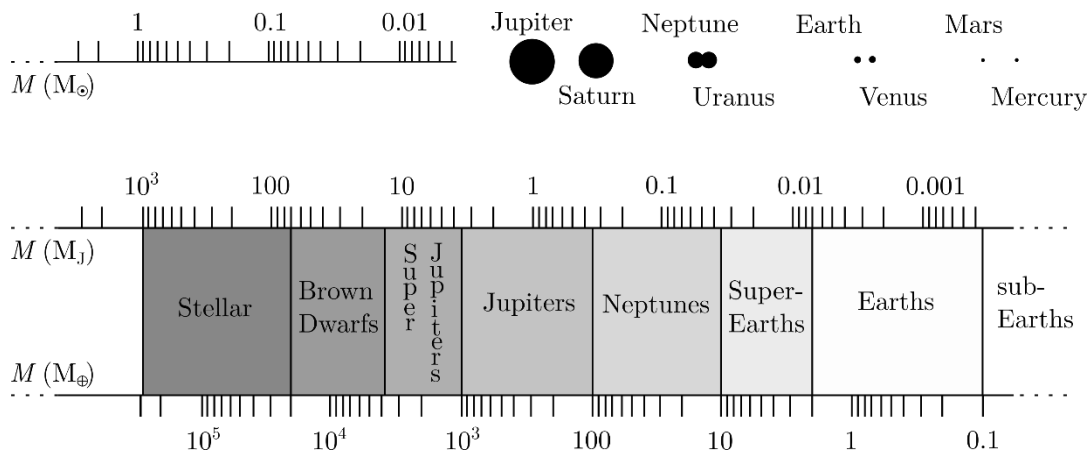
Figure 3.- Planet classification according to the mass of the object as proposed by Stevens and Gaudi (2013). Solar System objects are shown as an example. Figure from The Exoplanet Handbook by Michael Perryman (Perryman, 2018).

2.- SAMPLE

The dataset used in this work has been obtained with the CARMENES spectrograph installed at the 3.5m telescope at the Calar Alto observatory (Almería, Spain) that, since 2016, has obtained more than 15000 spectrums for 324 stars. It consists of time series of the radial velocity of each star including the epoch of observation, the radial velocity and its uncertainty. This sample (which is still being observed) is almost complete up to approximately 10 pc as can be seen in Figure 4, which shows the distribution of distances of our sample (Reiners et al. 2018b). For longer distances only the brightest early-type M-dwarfs stars can be observed.
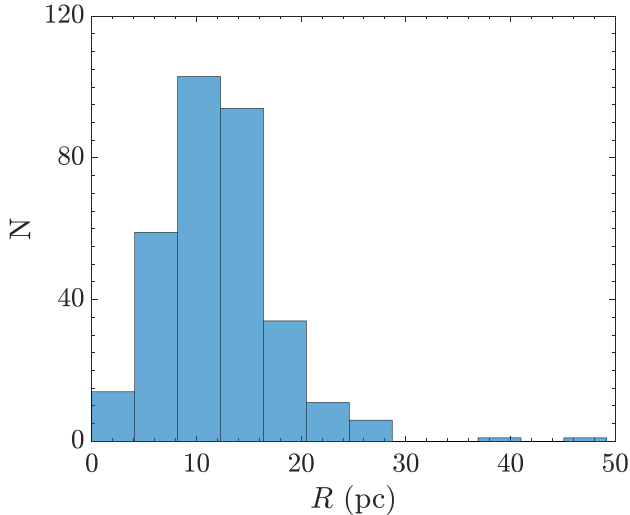
Figure 4.- Distribution of stars in the CARMENS sample as a function of distance (derived from parallax).

Figure 5 shows the distribution of stars as a function of the spectral type. Although the sample is especially rich in stars of type M3 to M4, it also includes all later-type stars up to M9. This enriches the sample, especially when compared to similar surveys such as HARPS, concentrated on earlier type stars.

Data is not annexed in this work due to confidentiality issues. It will be publicly available at the end of the CARMENES survey. The used dataset includes 324 radial velocity time series (one for each star). The total number of radial
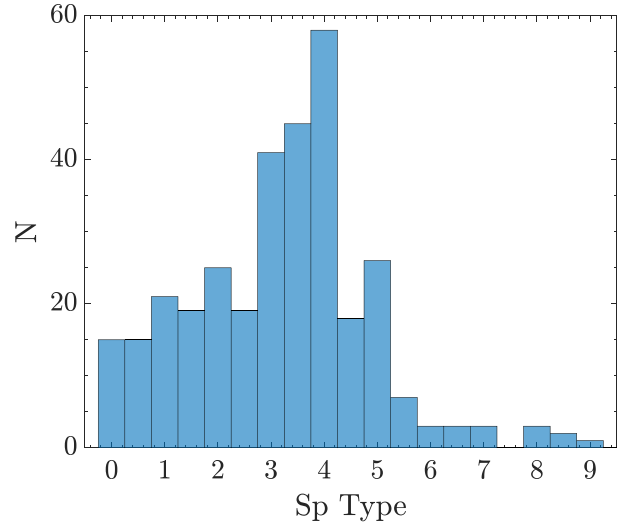
Figure 5.- Distribution of stars in the CARMENES sample as a function of the M Spectral Type (Sp Type).

velocities is 15467. The mean number of observations per star is 48. The less sampled star has only 4 radial velocity values yet while the more sampled star has 744. Figure 6 shows the dispersion of the radial velocity as a function of the J-band magnitude. As expected, stars fainter than $J \sim 9$ mag exhibit larger rms, due to the limitation of the CARMENES exposure time to 30 minutes. Several stars have also larger rms values that are related with real variability. The mean value of the radial velocity dispersion is $\sim$ 32 m/s, but this is largely dominated by the most active stars. The median value is $\sim$ 4 m/s.
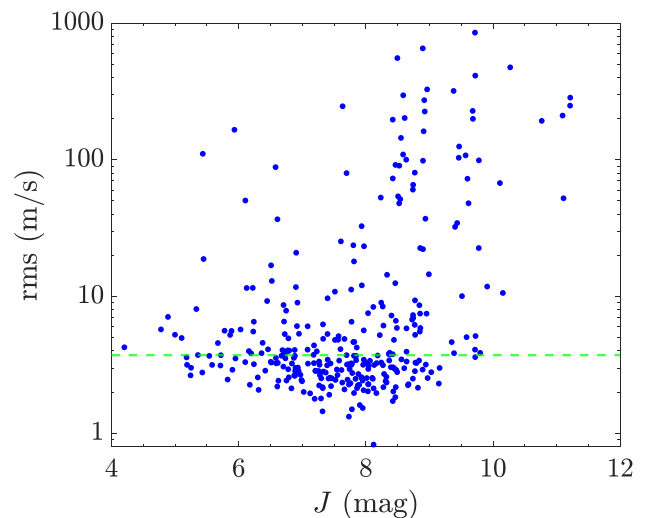

Figure 6.- J-band magnitude and rms for each of the 324 stars of the CARMENES sample. Green dashed line shows the median of the rms which has a value of 3.72 m/s.

3.- METHODS

To find the expected occurrence rate we need first to compute the detection limits, which depend on the instrumental noise of the radial velocities. This result allows us to discuss whether we can find more planets of the type that we are interested in with the current dataset, or if additional observations are needed. The followed process to compute the lower limit for the detection of variability is:

(i)   Periodic signal detection and computation of the residuals. We need a signal-clean sample as we are looking for the minimum detection within the instrumental noise.

(ii)   Noise analysis by introducing a sinusoidal signal associated with the presence of a planet. We increase the semi-amplitude (K) of the signal until it is detectable.

(iii)   Obtention of the associated minimum mass for each signal tested.

The estimation of the occurrence rate is computed after the obtention of the detection limits and is presented in Section 4. Next, we detail each step for the detection limit obtention to make it more comprehensible and reproducible. In Annex I an individual analysis for the first star of the sample (Star 1) can be found.

3.1.- VARIABILITY DETECTION

To study the planet occurrence rate, we need to first assess what are the detection limits, i.e., what planets can be detected with the current dataset. To do so, we need to look for periodic signals that may be associated both with the presence of planets or with the intrinsic variability of the star. Signals should be removed, as done when looking for exoplanets, so that we know what the level of instrumental noise of the timeseries of each dataset is. For the study of the

planet occurrence rate it is not necessary to identify the cause of the variability. However, during this study, several peaks were detected that could serve as a starting point for an exhaustive analysis of their origin. For instance, to confirm the planetary nature of this signals photometric variability can be checked to discard the signal being due to the imprint on radial velocities of spots caused by stellar activity on the surface of the star. If searching for a planet, we would need to create a model based on Kepler's laws to obtain the parameters in order to correctly fit the data.

To identify the signals in the data, we compute the periodogram of the time series looking for periodic signals. We use the generalized Lomb-Scargle periodogram (Zechmeister and Kürster, 2009), which is a generalization of the Lomb-Scargle periodogram (Scargle, 1982), with which we obtain more precise frequencies and are less susceptible to aliasing. As for the rest of the computations made in this work, the calculation of the periodogram was carried out using MATLAB computer software. As a result of the periodogram we obtain the power of each tested frequency, which can be understand as the importance of the frequency when modelling the data. Frequencies to be tested are chosen taking into account the observation time in which we have data on the radial velocity of the star (time of the final measure – time of the first measure), which we call t_{base}, and the number of measured data, N. This vector, of variable dimension depending on the parameters of the observation series of each star, therefore is composed as $f = 1/2t_{base} \cdot (1, 2, …, N)$.

There are different normalization methods for the powers of the periodogram. In order to maintain the same criteria throughout the process, we opted for a normalization to the variance of the sample so that the powers p meet $p \in [0, 1]$, being $p = 0$ a null improvement when

fitting the data and $p = 1$ a perfect fitting, since with this normalization p can be written as $p(f) = \left(\chi_0^2 - \chi^2(f)\right)/\chi_0^2$ (being $\chi^2(f)$ the minimum squared difference between the data and the model function and χ_0 the sample variance). The chosen normalization becomes important when estimating the false alarm probability (FAP) of a signal, which denotes the probability of a signal being produced just by chance. For our normalization, the power at which the FAP has a value FAP_{val} value is

$$FAP_p = 1 - \left(1 - (1 - FAP_{val})^{\frac{1}{M}}\right)^{\frac{2}{N-3}}, \quad (1)$$

(Zechmeister and Kürster, 2009) where M is the number of independent frequencies. This value can be estimated as the range of tested frequencies multiplied by the time range as $M = \left(f_{end} - f_{beg}\right) \cdot \left(t_{max} - t_{min}\right)$. We only consider as signals to subtract from our data those frequencies with a FAP $< 0.1\%$ as common in the exoplanets research field. As a result of this process we obtain a series of frequencies whose powers exceed the threshold power given by the 0.1% FAP.

As a first step to eliminate possible periodic signals from the data, we check in the literature whether the presence of any planet has been already announced for the star we are testing. In case that a planet is known, we check our data because its signal may not be detectable either because it has been filtered or because the discovery has been made with another instrument and it is not showing up in the CARMENES observations yet. In any of these cases we write down the characteristics of these planets and if we can detect them in our dataset, as we need that information to perform the occurrence rate analysis.

If we compute the periodogram and the signal is detected as a peak, we could now adjust the data to a periodic signal as

$$v_r = A + B \sin(2\pi t/P) + C \cos(2\pi t/P), \quad (2)$$

where P is the period of the planet and A, B and C fit parameters. Removing this signal, other peaks at the periodogram may disappear if they are harmonics or alias (frequencies resulting from the sampling method employed to collect data) simplifying the signal. The iterative process of fitting the data in a power descending order of the frequencies in the periodogram is known as pre-whitening. Pre-whitening's objective is to remove frequency peaks that are related to others, calculating the periodogram each time a periodic signal is removed. However, by fitting all the peaks at the same time, we obtain that those corresponding to aliases and harmonics of the main frequencies, result in negligible radial velocity amplitudes, not affecting the residuals of the time series. We obtain then a result compatible with the pre-whitening process, but the computational time is significantly reduced.

We therefore chose to compute the periodogram once at the beginning and fit data to a model

$$v_{model} = A + \sum_{i=1}^{n}[B_i \sin(2\pi f_i t) + C_i \cos(2\pi f_i t)], \quad (3)$$

where n is the number of frequencies, f_i, detected below the FAP $= 0.1\%$. If there is no peak detected, the measured data is assigned directly as noise. Parameters A, B and C are obtained from a fit to the measured values of the radial velocity and its uncertainty. Different routines were tested taking into account the uncertainty of each radial velocity value and also routines that did not consider it, obtaining similar results. We decided to use the 'lscov' routine, from Least-squares solution in presence of known covariance, (Strang, 1986), due to its agility, precision, and consideration of uncertainties. Once the fit parameters were estimated, we proceeded to remove the signal from the sample, assuming then that data residuals are associated with instrumental noise.

For some stars in the sample, it is necessary to carry out an individual analysis with some previous considerations. These cases include stars in which the data was taken in a continuous way (obtaining many values per night) and stars with very long periods where the effects of the window of observation in the periodogram (window function) or the possibility of having signals with periods larger than the observations timespan. In the first case, we averaged the observations for each night. This greatly simplified the data allowing a correct interpretation of the periodogram with a better frequency selection. In the second case, we made a parametric sinusoidal fit considering long periods. Examples of long-period signal stars can be found in Annex II, where we also provide an estimation of the periods found.

3.2.- DETECTION LIMITS

Once all possible exoplanet and stellar signals are removed, we assume the remaining data is only due to stellar jitter (non-periodic variability) or instrumental noise, which limits the kind of planets we can detect. Thus, we estimate what would be the smallest signal that we could detect with this level of radial velocity noise. That is, we look for the smallest radial velocity semi-amplitude that we can detect between the noise for each frequency value. The frequencies that we test in this case differ from the previous ones since we need a common frequency vector for all the stars. We test periods between 2 and 2400 days (median of the maximum detectable periods that we reach in the individual sampling of each star). Hence, we sample the frequency range between at $1/2400$ days^{-1} and $1/2$ days^{-1}, with two different steps, f_s and $3f_s$, for frequencies smaller and larger than $1/50$ days^{-1}, respectively, where $f_s = 1/2400$ days^{-1}. With this vector of frequencies, we can test the interval of periods in which we are interested, mainly Jupiter- and Neptune-like planets in long orbits, finding a balance between precision, the

number of tested frequencies, and computational time. Next, we compute the periodogram to obtain the power p of each of these frequencies that is associated with the noise. We do this 1000 times reordering randomly the data each time, obtaining a vector of 1000 powers for each frequency, all of them compatible with noise.

Then, we introduce a mock signal in the time series as $\widehat{v_r} = K \cdot \cos(2\pi f t + \phi)$ (m/s). When introducing this signal, we are assuming a zero-eccentricity orbit, which is a good approximation for eccentricities as high as 0.5 (Cumming & Dragomir, 2010; Bonfils, 2013). We choose the initial testing semi-amplitude at each frequency at those corresponding to the best sinusoidal fit to the time series. We compute the periodogram of the composed data and estimate the significance of this mock signal as the fraction of times that its power exceeds the noise power for each frequency computed above. We keep increasing the semi-amplitude value until this percentage is above 99%. This process is equivalent to calculate detection with a 1% FAP. We repeat this process for 12 equi-spaced radial velocity phase (ϕ) values averaging all obtained K. We carry out the same process for all the frequencies and all the stars. With this we obtain the minimum value of K that is detected at each frequency f. This process supposes about 250 hours of calculation in a computer with standard characteristics (computer with 4 cores at 3.40 GHz and 16 Gb of RAM), and strongly depends on the choice of the testing frequencies vector.

3.3.- MINIMUM MASS COMPUTATION

To obtain the minimum mass of the planet that we could detect, or what is the same, the detection threshold mass, for each period we need to convert the amplitudes of the signal into the mass of the planet multiplied by its inclination. For this we assume that the mass of the planet is much smaller than the mass of the host star (in

addition to the zero-eccentricity approximation). Therefore, from Equation 1 of Cumming et al. (1999):

$$K = \left(\frac{2\pi G}{P}\right)^{1/3} \frac{m\sin i}{(M_* + m)^{2/3}} \frac{1}{(1-e^2)^{1/2}}, \qquad (4)$$

we derive the expression from which we computed the minimum mass as

$$K \approx \left(\frac{2\pi G}{P}\right)^{1/3} \frac{m\sin i}{M_*^{2/3}}, \qquad (5)$$

where M_* is the mass of the host star, i the orbital inclination with respect of the line of sight, m the planet mass, and P the orbital period. Combining the possible detected planets for the noise of each star we can calculate the percentages of planets that we expect for each period and mass since we know those that have already been detected previously.

4.- RESULTS AND DISCUSSION

Table 1 shows the 61 known planets orbiting stars in our sample. Due to confidentially issues, the real name of planetary firm candidates still under investigation and not published are omitted. Of these 61 planets, 35 have been discovered by CARMENES or they are detected in the data but previously announced by other exoplanet surveys.

After removing the significant signals in the periodogram, we calculate the detection limits for each star in the sample. The limits for each star are shown in Figure 7. This figure, more than only being useful as a first visual control of the results, allows us to check the interval of minimum planetary masses that can be detected. We see that the greater the mass and the shorter the period, the lower the detection limit. We can obtain more information by drawing the different quantiles as shown in Figure 8. Quantiles divide the diagram into detection probability zones allowing us to make more powerful interpretations

such as the percentage of stars in whose noise data we could not discern a certain planet. Thus, for instance the 75th quantile tells us that, for the CARMENES dataset under study, planets with $m\sin i$ greater than this value would be detected in 75% of stars from our sample. We see that, for periods less than 1000 days, CARMENES is sensitive to 70% of the Jupiter and Neptune-type planets and that the GJ3512b-type planets ($m \cdot \sin i \sim 147.1\,M_\oplus$, $P = 203.59$ days) would have been found around more than 80% of the stars if existing.
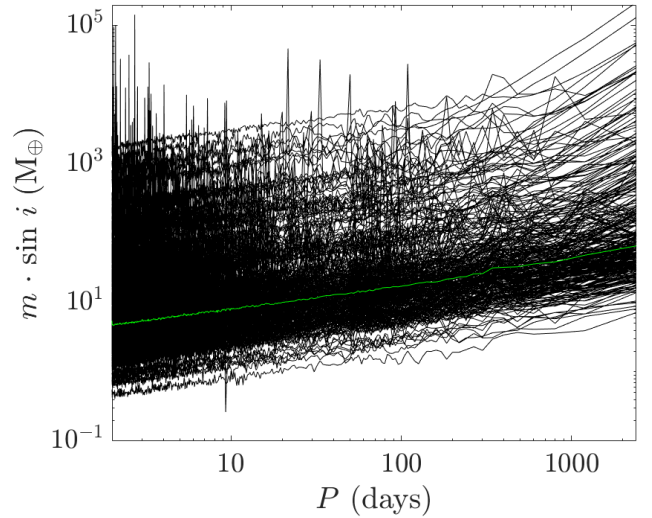
Figure 7.- Computed detection limits for the 324 stars of the CARMENES dataset. Green solid line traces the median. We see how the greater the mass and the shorter the period, the lower the detection limit.

The computed detection limits and the corresponding quantiles give the survey efficiency, which is used to derive the occurrence rate of planets around M-dwarf stars taking into account the detection incompleteness of the survey. To do this, we consider, together with the detection limits, the list of planets that are detected around the stars in the sample. We can estimate the occurrence rate for a certain group of planets by dividing the number of detected planets in this group, N_d, over the number of stars whose detection limits confidently tell us that all such planets would have been detected, N_s. We estimate N_s from the number of stars in our sample, $N_T = 324$, and the average probability of

Table 1.- Exoplanets discovered around the 324-stars CARMENES M dwarf sample. The name of the planet, orbital period (P), minimum planet mass ($m \sin i$), host-star mass (M_*), spectral type (Sp Type) and discovery bibliographic reference are listed. The real name of CARMENES firm planet candidates not yet published is omitted for confidentially issues.

| Name	P (days)	$m \cdot \sin i$ (M$_\oplus$)	M_*(M$_\odot$)	Sp Type	References
GJ 229 b	471.00	32.00	0.53	M0.5	Tuomi et al., 2014
GJ 876 b	61.07	623.84	0.33	M4	Correia et al., 2010
c	30.26	252.70			
d	1.94	15.36			
GJ 317 b	692.00	82.24	0.42	M3.5	Anglada-Escudé et al., 2012
LSPM J2116+0234 b	14.44	13.28	0.43	M3	Lalitha et al., 2019
GJ 581 b	5.37	15.65	0.30	M3	Mayor et al., 2009
c	12.93	5.36			
d	66.80	7.09			
e	3.15	1.94			
GJ 179 b	2288.00	260.61	0.36	M3.5	Howard et al., 2010
GJ 447 b	9.90	1.35	0.18	M4	Bonfils et al., 2018
HD 147379 b	86.54	25.00	0.63	M0	Reiners et al., 2018a
Teegarden b	4.91	1.05	0.09	M7	Zechmeister et al., 2019
c	11.41	1.11			
GJ 1148 b	41.38	96.70	0.35	M4	Trifonov et al., 2018
c	532.58	68.06			
Star 86 b	2.91	3.95			Bauer et al., 2020
Star 96 b	9.03	6.50			
Barnard b	232.80	3.23	0.17	M3.5	Ribas et al., 2018
GJ 180 b	17.38	8.30	0.41	M2	Tuomi et al., 2014
c	24.33	6.40			
GJ 436 b	2.64	21.00	0.43	M2.5	Butler et al., 2004
HD 180617 b	105.90	12.20	0.48	M2.5	Kaminski et al., 2018
GJ 3779 b	3.02	8.00	0.27	M4	Luque et al., 2018
GJ 687 b	38.14	18.00	0.41	M3	Burt et al., 2014
GJ 536 b	8.70	5.36	0.50	M1	Suarez-Mascareno et al., 2017
Star 180 b	698.72	106.20	0.50	M1	
Wolf 1061 b	4.89	1.33	0.29	M3.5	Wright et al., 2016
c	17.87	4.10			
d	67.28	4.97			
AD Leo b	2.22	19.70	0.44	M3	Tuomi et al., 2018
GJ 1265 b	3.65	7.40	0.18	M4.5	Luque et al., 2018
GJ 3543 b	1.12	2.60	0.47	M1.5	Astudillo-Defru et al., 2017
Star 193 b	14.23	4.00	0.36	M3	
GJ 378 b	3.82	13.02	0.58	M1	Hobson et al., 2019
GJ 273 b	18.65	2.89	0.30	M3.5	Astudillo-Defru et al., 2017
c	4.72	1.18			
Star 203 b	13.68	7.00	0.58	M0	
HD 79211 b	24.40	9.15	0.59	M0	González Álvarez et al., 2020
GJ 649 b	598.30	104.24	0.51	M1	Johnson et al., 2009
GJ 3512 b	203.59	147.15	0.12	M5.5	Morales et al., 2019
Star 246 b	15.56	1.60	0.16	M5	
Star 250 b	8.05	4.00	0.30	M4	
GJ 686 b	15.53	6.50	0.43	M1	Affer et al., 2019; Lalitha et al., 2019
GJ 15A b	7592.00	36.00	0.39	M1	Pinamonti et al., 2018
c	11.40	3.03			
GJ 176 b	8.70	8.40	0.50	M2	Bonfils et al., 2013
GJ 625 b	14.60	2.82	0.32	M1.5	Suarez Mascareno et al., 2017
GJ 411 b	13.00	2.99	0.35	M1.5	Diaz et al., 2019
GJ 849 b	18.00	310.00	0.47	M3.5	Bonfils et al., 2013
Star 293 b	765.94	75.70	0.15	M3.5	
GJ 49 b	13.85	5.63	0.52	M1.5	Perger et al., 2019
GJ 3323 b	5.36	2.02	0.17	M4	Astudillo-Defru et al., 2017
c	40.54	2.31			
YZ Cet b	1.97	0.75	0.14	M4.5	Astudillo-Defru et al., 2017;
c	3.06	0.98			Stock et al., 2020
d	4.66	1.14			
Star 321 b	36.03	6.10	0.28	M4	
GJ 4276 b	13.35	15.58	0.41	M4	Nagel et al., 2019
c	6.68	4.40			
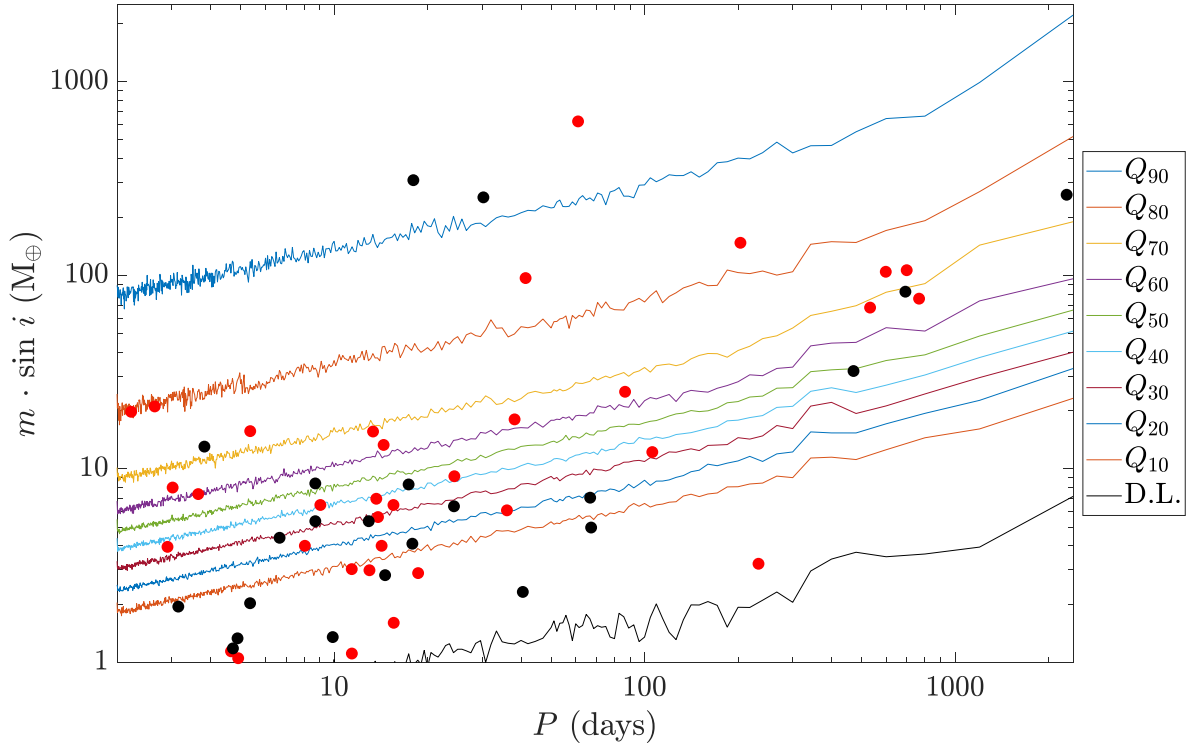
Figure 8.- Detection limit quantiles for all the stars in the CARMENES sample, as a function of the orbital periods. The 90th to 10th quantiles are drawn in different colours as labelled. Black solid line shows the lowest mass detection limit (D.L.). Red dots correspond to planets that have either been discovered by CARMENES or whose signal is present in the time series. Black dots correspond to other exoplanets orbiting around host stars of our dataset, but for which data is not enough to claim detection. We only use the first for the occurrence rate estimation.

detection in the considered mass and period range. To calculate this probability, we simulate 10^5 planets assuming a log-uniform probability for $m \sin i$ and P. For each of these simulated planets we calculate its probability of detection with respect to the closest quantile.

For each probability we calculate a value for N_s with which an occurrence rate is estimated. In order to have statistically significant values, we divide our parameter space in different planetary mass ranges approximately matching super-Earth $(1 - 10)$ $M_\oplus$, Neptune-like $(10 - 100)$ $M_\oplus$, and Jupiter-like $(100 - 1000)$ $M_\oplus$ planets. We also use three period ranges: $2 - 10$, $10 - 100$, and $100 - 1000$ days. For each range, we estimate the 1σ quantiles in that area of the diagram. We caution here the reader that we are mainly interested in the values of Neptune and Jupiter-like planets. We also provide for completeness the occurrence rates for super-Earth like planets $(1 - 10)$ $M_\oplus$, but

these values should be taken with caution because they encompass our lowest detection limits as shown in Figure 8. Particularly for periods longer than 10 days there are regions where $N_s = 0$, that means it is an excluded region by the detection limit. To avoid this regions were our survey is not sensitive to planets, we only count the simulated planets above a threshold $N_s \geq 0.01$ N_T (first quantile). Table 2 summarize the results for the different plant mass and period ranges. N_d and N_s are shown with the occurrence rate for each group.

We can compare our results with those obtained by other exoplanet surveys focused on M-dwarf stars. For instance, Clanton and Gaudi (2016) estimate planetary occurrence rates from microlensing (Gould et al. 2010, Sumi et al. 2010), and radial velocity surveys (HARPS RV survey, Bonfils et al., 2013). The results of this work are listed in Table 3.

Table 2.- Occurrence rate (in percentage, i.e., number of planets per 100 stars) of the different groups of planets obtained from the analysis of the CARMENES 324 stars. N_d indicates the number of planets discovered by CARMENES or showing significant signals in the timeseries data. N_s indicates the average number of stars whose detection limits confidently tell us that all such planets would have been detected in each range. For 1–10 $M_\oplus$, N_s is best estimated as the median of the computed values in each group. (*2σ limit is given due to low statistics).

$m \sin i$ ($M_\oplus$)	P (days)		
	$2 - 10$	$10 - 100$	$100 - 1000$
$100 - 1000$	< 0.33 $N_d = 0$ $N_s = 304$	$0.34^{+0.02*}_{-0.02}$ $N_d = 1$ $N_s = 298$	$1.09^{+0.07}_{-0.06}$ $N_d = 3$ $N_s = 279$
$10 - 100$	$1.16^{+0.08}_{-0.07}$ $N_d = 3$ $N_s = 260$	$2.06^{+0.50}_{-0.13}$ $N_d = 5$ $N_s = 230$	$1.68^{+2.02}_{-0.36}$ $N_d = 3$ $N_s = 162$
$1 - 10$	10^{+32}_{-6} $N_d = 7$ $N_s = 65$	68^{+271}_{-54} $N_d = 11$ $N_s = 16$	31^{+1*}_{-24} $N_d = 1$ $N_s = 3$

Table 3.- Planet occurrence rate measured by radial velocity and microlensing surveys (Clanton and Gaudi, 2016). For periods from 1 to 100 days, occurrence rate is computed only from radial velocity data from HARPS. For periods from 100 to 1000 days data from microlensing surveys is used.

$m \sin i$ ($M_\oplus$)	P (days)		
	$1 - 10$	$10 - 100$	$100 - 1000$
$100 - 1000$	< 1 $N_d = 0$	2 $N_d = 2$	< 1
$10 - 100$	3 $N_d = 2$	< 2 $N_d = 0$	$> 2.0 \pm 0.9$ < 4
$1 - 10$	36 $N_d = 5$	52 $N_d = 3$	$> 8 \pm 3$

We highlight here some interesting results. First, detections are achieved in 8 of the 9 considered ranges. This is an improvement with respect the results shown in Table 3, where for 5

of the mass-periods ranges only lower or upper levels are obtained. As mentioned, the large uncertainty obtained in the mass range between 1 and 10 $M_\oplus$ is due to the lower detection probability of this system, which may increase as the survey progresses. The comparison in this mass regime is thus complex and we should wait to the completion of the survey to reach firm conclusions. However, it is interesting to note that, for the first time, CARMENES provides some statistics of super-Earths at periods longer than 100 days using radial velocities. In this range we only obtain $N_s = 3$ stars. This limitation on the number, restricts the statistics obtained and cause large uncertainties; but interestingly, the mean value is consistent with the lower limit obtained from the microlensing survey analysis ($> 8 \pm 3$ %). Second, these results seem to confirm the observed reduced number of planets with masses and periods lower than 10 $M_\oplus$ and 10 days, with respect longer periods. The analysis of HARPS data (Bonfils et al. 2013) reported a super-Earth occurrence rate of 36% and 52% for periods below and above 10 days, respectively. Our CARMENES data, results in 10% and 68% for the same period ranges, showing a bigger difference between them. Exoplanet statistics coming from transiting surveys do also show the same trend (Dressing and Charbonneau 2015). Formation models should explain this pheno-menon, which may be due to a reduced efficiency forming planets at shorter distances of the host star, or of the migration mechanisms in this innermost region.

Finally, regarding higher mass planets, CARMENES reveals a larger occurrence rate of such planets at long period orbits than former radial velocity studies (Bonfils et al., 2013). A total of 3 planets more massive than 100 $M_\oplus$ and with periods between 100 and 1000 days, including GJ 3512b, have been detected. This allows to obtain an occurrence rate of 1.09%. This

is close to the upper limit of 1% obtained by combining microlensing and radial velocity surveys, which may arise from the small number of stars studied and the low-occurrence rate. The detection efficiency of CARMENES in the Neptune- and Jupiter-like planets range can be clearly seen in Figure 8. For masses greater than 10 $M_\oplus$ approximately 70% of the planets are observable by CARMENES.

To further exploit the characteristics of our sample, we decided to analyse the occurrence rate according to the mass of the host star. As Figure 9 shows, the mass of the observed stars, ranges from 0.05 to 0.75 $M_\odot$. We divide the sample into stars with masses larger or smaller than 0.25 $M_\odot$. This would be approximately equivalent to having two subsamples, one with stars of spectral type M0 to M3 and the other with stars of type M4 and later.
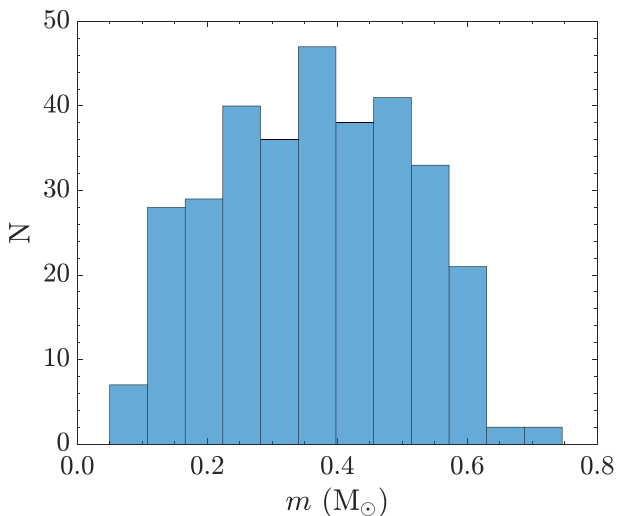

Figure 9.- Distribution of stars in the CARMENES sample as a function of their mass.

The process followed to calculate the occurrence rate in these two subsamples does not differ from that explained above. The only difference is that, as the number of stars per subsample changes, there is a lack of detected planets in some ranges, especially for the smallest sample, the one with masses smaller than 0.25 $M_\odot$. Table 4 list the results obtained for the lower

stellar mass subsample, which consist on 73 stars around which 9 planets have been discovered. We only compute occurrence rates for ranges of planet mass and orbital period where some planet has been detected, but upper limits are given considering $N_d < 1$ in the other regions.

Table 4.- Occurrence rate (in percentage, i.e., number of planets per 100 stars) of the different groups of planets obtained from the analysis of the CARMENES stars with $M_* < 0.25$ $M_\odot$. N_d indicates the number of detected planets in the CARMENES survey. N_s corresponds to the average number of stars where planets in this mass and period ranges would have been detected according to detection limits.

$m \sin i$ ($M_\oplus$)	P (days)		
	$2 - 10$	$10 - 100$	$100 - 1000$
$100 - 1000$	< 1.4 $N_d = 0$ $N_s = 71$	< 1.5 $N_d = 0$ $N_s = 68$	$1.61^{+0.20}_{-0.17}$ $N_d = 1$ $N_s = 62$
$10 - 100$	< 1.8 $N_d = 0$ $N_s = 55$	< 2.0 $N_d = 0$ $N_s = 50$	$2.49^{+1.4}_{-0.4}$ $N_d = 1$ $N_s = 39$
$1 - 10$	16^{+39}_{-6} $N_d = 4$ $N_s = 26$	18^{+36}_{-11} $N_d = 2$ $N_s = 11$	14^{+120}_{-5} $N_d = 1$ $N_s = 7$

The ranges in which we have been able to estimate the occurrence rate are interesting, especially those corresponding to long periods ones. Stars in this subsample have smaller masses, thus they are also more sensitive to disturbances produced by planets with small mass or with longer periods. In the range of masses from 1 to 10 $M_\oplus$ we can observe planets in all ranges of periods. If we now look at planets with masses larger than 100 $M_\oplus$ and long periods (100 - 1000 days), we obtain $N_s = 62$ stars, which, compared to the total number of stars in the subsample, is an indicator of a high probability of detection. This combined with the detection of a planet (GJ 3512b) gives us an occurrence rate of 1.61%. Interestingly, no giant planets at periods between

10 and 100 days are found, even though they should be easily identified. Although larger statistics are needed to draw firm conclusions, this may point towards an increase of the efficiency forming planets around very-low mass stars at larger distances, where gravitational instability may be at play.

Table 5 summarizes the results obtained for the subsample with stars more massive than 0.25 M$_\odot$. In this case the subsample size increases to 251 stars around which 25 planets have been discovered. For comparison, the HARPS spectrograph has observed about 100 stars in this same range. Thus, CARMENES increases considerably the statistical significance of the occurrence rates. Focusing on the computed values, we obtained results more in agreement with those reported by Clanton and Gaudi (2016) for massive long-term planets. Again, we obtain a much lower occurrence rate for the 1 to 10 M$_\oplus$ with short period than that computed by other surveys, that may improve as the survey evolves. Interestingly, a slightly larger occurrence rate of Jupiter and Neptune-like planets at long period orbits is found around less massive stars, although these results need to be confirmed increasing the statistics of observed stars.

5.- CONCLUSION

We derived the planet occurrence rate around M-dwarf stars, for different ranges of mass and period, using the radial velocity data from the CARMENES survey and analysing the detection limits for each star. Driven by the discovery of the GJ3512b system, a giant exo-planet orbiting a very late-type star, we focused our attention into Jupiter-like planets. We have obtained that the occurrence rate of planets with masses between 100 and 1000 M$_\oplus$ with periods between 100 days and 1000 days is approximately 1%. Furthermore,

Table 5.- Occurrence rate (in percentage, i.e., number of planets per 100 stars) of the different groups of planets obtained from the analysis of the CARMENES stars with $M_* > 0.25$ M$_\odot$. N_d indicates the number of detected planets in the CARMENES survey. N_s corresponds to the average number of stars which can detect planets in each range. (*2σ limit is given as 1σ = 0).

$m \sin i$ (M$_\oplus$)	P (days)		
	2 – 10	10 – 100	100 – 1000
100 –1000	< 0.42 $N_d = 0$ $N_s = 234$	$0.44^{+0.03*}_{-0.023}$ $N_d = 1$ $N_s = 229$	$0.94^{+0.12*}_{-0.05}$ $N_d = 2$ $N_s = 217$
10 – 100	$1.41^{+0.18}_{-}$ $N_d = 3$ $N_s = 205$	$2.65^{+0.66}_{-0.31}$ $N_d = 5$ $N_s = 181$	$1.44^{+2.54}_{-0.38}$ $N_d = 2$ $N_s = 124$
1 – 10	5^{+19}_{-3} $N_d = 3$ $N_s = 63$	24^{+47}_{-12} $N_d = 9$ $N_s = 38$	< 8 $N_d = 0$ $N_s = 13$

when dividing our sample according to the mass of the host stars we obtained that this number is slightly larger for the lower mass M-dwarfs. The formation of such kind of planetary systems, is more easily explained by the gravitational instability model, instead of core accretion mechanism. This occurrence rate difference thus may point that GJ 3512b may not be an exception, but that gravitational instability may be at play in some cases, probably depending on the properties of the protoplanetary disk and the host star, yielding a different planet population. We were also able to estimate the occurrence rate for super-Earths with long periods giving a value of $\sim 30\%$. This value agrees well with the upper limit estimated from microlensing survey analysis, but it is obtained from radial velocity data for the first time.

There are different sections in this project where there is room for improvement allowing better estimates. We could increase the range of

periods tested during the detection limits and use a denser grid of frequencies. For this work this was not possible due to the long computer time that it supposes. It will also be interesting to repeat the estimates for the occurrence rate once the survey is finished with the aim of reporting a final result to the CARMENES detections, in particular for the smaller range of planetary masses, for which the detection limits are still prone to improvement with further observations.

ACKNOWLEDGEMENTS

REFERENCES

Affer, L. et al. (2019) "HADES RV program with HARPS-N at the TNG. IX.- A super-Earth around the M dwarf Gl 686" in *Astronomy and Astrophysics*. Vol. 622, A193. 2019 February.

Anglada-Escudé, G. et al. (2012) "Astrometry and Radial Velocities of The Planet Host M Dwarf GJ 317: New Trigonometric Distance, Metallicity, And Upper Limit to the Mass of GJ 317b" in *The Astrophysical Journal*, Vol 746 pp. 37-51. 2012 February.

Astudillo-Defru, N. et al. (2015) "The HARPS search for southern extra-solar planets XXXVI. Planetary systems and stellar activity of the M dwarfs GJ 3293, GJ 3341, and GJ 3543" in *Astronomy and Astrophysics*. Vol 575. 2015.

Astudillo-Defru, N. et al. (2017) "The HARPS search for southern extra-solar planets XLI. A dozen planets around the M dwarfs GJ 3138, GJ 3323, GJ 273, GJ 628, and GJ 3293" in *Astronomy and Astrophysics*. Vol 602. 2017 June.

Astudillo-Defru, N. et al. (2017) "The HARPS search for southern extra-solar planets XLII. A system of Earth-mass planets around the nearby M dwarf YZ Ceti" in *Astronomy and Astrophysics*. Vol 605, letter 11. 2017 September.

Bakos, G. et al. (2004) "Wide-Field Millimagnitude Photometry with the HAT: A Tool for Extrasolar Planet Detection" in *Publications of the Astronomical Society of the Pacific*. Vol. 116 p.817. 2004.

Bauer, F.F. et al. (2020) "The CARMENES search for exoplanets around M dwarfs. Measuring precise radial velocities in the near infrared: the example of the super-Earth CD Cet b" in *Astronomy and Astrophysics*. Vol and pages to be concreted. 2020 June

Berta, Z.K. et al. (2012) "Transit Detection in the MEarth Survey of Nearby M Dwarfs: Bridging the Clean-first, Search-later Divide" in *The Astronomical Journal*. Vol 144, 20 pp. 2012 November.

Bonfils, X. et al. (2018) "A temperate exo-Earth around a quiet M dwarf at 3.4 parsec" in *Astronomy and Astrophysics*. Vol 613. 2018.

Bonfils, X. et al. (2013) "The HARPS search for southern extra-solar planets. XXXI.- The M-dwarf sample" *in Astronomy and Astrophysics*. Vol. 549. 2013 January.

Borucki, J.W. et al. (2011) "Characteristics of Planetary Candidates Observed by Kepler. Ii. Analysis of The First Four Months of Data" in *The Astrophysical Journal*. Vol. 736, Number 1. 2011 June.

Boss, A. P. (1997) "Giant planet formation by gravitational instability." in *Science*, Vol. 276, p. 1836-1839 (1997).

Brouwers, M.G. et al. (2018) "How cores grow by pebble accretion" in *Astronomy and Astrophysics*. Vol. 611. 2018.

Burt, J et al. (2014) "The Lick–Carnegie Exoplanet Survey: Gliese 687b—A Neptune-Mass Planet Orbiting a Nearby Red Dwarf" in *The Astrophysical Journal*. Vol 789, pp. 114-128. 2014 July.

Butler, R.P. et al. (2004) "A Neptune-Mass Planet Orbiting the Nearby M Dwarf GJ 436" in *The Astrophysical Journal*. Vol. 617, pp. 580-588. 2004 December.

Cameron, A. G. W. (1978) "Physics of the Primitive Solar Accretion Disk" *The Moon and the Planets*, Volume 18, Issue 1, pp.5-40. February 1978

Clanton, C. and Gaudi, B.S. (2016) "Synthesizing Exoplanet Demographics: A Single Population of Long-Period Planetary Companions to M Dwarfs Consistent with Microlensing, Radial Velocity, And Direct Imaging Surveys" in *The Astrophysical Journal.* Vol 819, pp. 125-167. 2016 March.

Cochran, W.D. et al. (1991) "Constraints on the companion object to HD 114762" in *The Astrophysical Journal.* Vol. 380. 1991 October.

Correia, A.C.M et al. (2010) "The HARPS search for southern extra-solar planets. XIX.- Characterization and dynamics of the GJ 876 planetary system" in *Astronomy and Astrophysics.* Vol 511. 2010.

Cumming, A. and Dragomir, D. (2010) "An integrated analysis of radial velocities in planet searches" in *Monthly Notices of the Royal Astronomical Society.* Vol. 401, pp. 1029-1042. 2010 January.

Diaz, R.F. et al. (2019) "The SOPHIE search for northern extrasolar planets. XIV.- A temperate (T_{eq} 300 K) super-earth around the nearby star Gliese 411" in *Astronomy & Astrophysics.* Vol. 625. 2019 May.

Dressing, C.D. and Charbonneau, D. (2015) "The Occurrence of Potentially Habitable Planets Orbiting M Dwarfs Estimated from the Full Kepler Dataset and an Empirical Measurement of the Detection Sensitivity" in The Astrophysical Journal. Vol. 807, N 45. 2015 July.

Fischer, D.A. et al. (2014) "Exoplanet Detection Techniques" in *Protostars and Planets VI.* Publisher: University of Arizona Press. 2014.

González-Álvarez, E. et al. (2020) "The CARMENES search for exoplanets around M dwarfs. A super-Earth planet orbiting HD 79211 (GJ 338 B)" in *Astronomy and Astrophysics.* Vol 637. 2020 May.

Gould, A. et al. (2010) "Frequency of Solar-Like Systems and of Ice and Gas Giants Beyond the Snow Line from High-Magnification Microlensing Events In 2005-2008" in *The Astrophysical Journal.* Vol. 270, number 2. 2010 August.

Hobson, M.J. et al. (2019) "The SOPHIE search for northern extrasolar planets. XV.- A warm Neptune around the M dwarf Gl 378" in *Astronomy and Astrophysics.* Vol 625. 2019.

Howard, A. W. et al. (2010) "The California Planet Survey. I. Four New Giant Exoplanets" in *The Astrophysical Journal.* Vol 721 pp. 1467-1481. 2010 October.

IEEC (2019) "CARMENES: Giant exoplanet around a small star challenges our understanding of how planets form" [Press release]. 2019 September. Accessed on June 2020 at http://www.ieec.cat/en/content/58/news/detail/791/carmenes-giant-exoplanet-around-a-small-star-challenges-our-understanding-of-how-planets-form

Johansen, A. and Lambrechts, M. (2017) "Forming Planets via Pebble Accretion" *in Annual Review of Earth and Planetary Science.* 2017. 45:359–87. 2017.

Johnson, J.A. et al. (2009) "The California Planet Survey. II. A Saturn-Mass Planet Orbiting the M Dwarf Gl 649" in *Publications of the Astronomical Society of the Pacific.* Vol 122, pp. 149-155. 2010 February.

Kaminski, A. et al. (2018) "The CARMENES search for exoplanets around M dwarfs. A Neptune-mass planet traversing the habitable zone around HD180617" in *Astronomy and Astrophysics.* Vol 618. 2018.

Kuiper, G.P. (1951) "On the Origin of the Solar System" in *Proceedings of the National Academy of Sciences of the United States of America*, Volume 37, Issue 1, 1951, pp.1-14. January 1951.

Lalitha, S. et al. (2019) "The CARMENES search for exoplanets around M dwarfs. Detection of a mini-Neptune around LSPM J2116+0234 and refinement of orbital parameters of a super-Earth around GJ 686 (BD+18 3421)" in *Astronomy and Astrophysics.* Vol 627. 2019.

Lambrechts et al. (2014) "Separating gas-giant and ice-giant planets by halting pebble accretion" in *Astronomy and Astrophysics.* Vol. 572. 2014 December

Lambrechts, M. and Johansen, A. (2012) "Rapid growth of gas-giant cores by pebble accretion" in *Astronomy and Astrophysics.* Vol. 544. 2012 August.

Latham, D. W. et al. (1989) "The unseen companion of HD114762: a probable brown dwarf" in *Nature.* Vol. 339, pp. 38–40. 1989.

Lissauer, J.J. (1993) "Planet formation" *in Annual Review of Astronomy and Astrophysics.* Vol. 31, pp. 129-174. 1993.

Luque, R. et al. (2018) "The CARMENES search for exoplanets around M dwarfs. The warm super-Earths in twin orbits around the mid-type M dwarfs Ross 1020 (GJ 3779) and LP 819-052 (GJ 1265)" in *Astronomy and Astrophysics.* Vol 620. 2018.

Mayor, M et al. (2009) "The HARPS search for southern extra-solar planets. XVIII.- An Earth-mass planet in the GJ 581 planetary system" in *Astronomy and Astrophysics.* Vol 507 pp. 487-494. 2009.

Mayor, M. et al. (2003) "Setting New Standards with HARPS" in *The Messenger.* N 114, pp. 20-24. 2003 December.

Mayor, M., and Queloz, D. (1995). A Jupiter-mass companion to a solar-type star. *Nature.* Vol. 378, pp. 355–359. 1995.

Morales, J.C. et al. (2019) "A giant exoplanet orbiting a very-low-mass star challenges planet formation models" in *Science.* Vol 635. 2019 September.

Nagel, E. et al. (2019) "The CARMENES search for exoplanets around M dwarfs. The enigmatic planetary system GJ 4276: one eccentric planet or two planets in a 2:1 resonance?" in *Astronomy and Astrophysics.* Vol 622. 2019.

NASA Exoplanet Archive (2020) "Exoplanet exploration. Planets Beyond Our Solar System". In https://exoplanetarchive.ipac.caltech.edu/.Accesed on June 2020.

Ormel, C.W. and Klahr, H.H. (2010) "The effect of gas drag on the growth of protoplanets. Analytical expressions for the accretion of small bodies in laminar disks" in *Astronomy and Astrophysics.* Vol. 520. 2010 September.

Perger, M. et al. (2019) "Gliese 49: activity evolution and detection of a super-Earth A HADES and CARMENES collaboration" in *Astronomy and Astrophysics.* Vol. 624. 2019.

Perryman, M. (2018) "The Exoplanet Handbook". Publisher: Cambridge University Press. ISBN 9781108419772. 2018.

Pinamonti, M. et al. (2018) "The HADES RV Programme with HARPS-N at TNG. VIII. GJ15A: a multiple wide planetary system sculpted by binary interaction" in *Astronomy & Astrophysics.* Vol. 617. 2018 September.

Pollacco, D.L. et al. (2006) "The WASP Project and the SuperWASP Cameras" in *Publications of the Astronomical Society of the Pacific.* Vol 118, pp. 1407–1418. 2006 October

Pollack, J.B. et al. (1996) "Formation of the Giant Planets by Concurrent Accretion of Solids and Gas" in *Icarus.* Vol. 124, pp. 62-85. 1996 November.

Quirrenbach, A. et al. (2014) "CARMENES instrument overview" in *Proceedings of the SPIE.* Vol. 9147. 2014 July.

Ranalli, P. et al. (2018) "Astrometry and exoplanets in the Gaia era: a Bayesian approach to detection and parameter recovery" in *Astronomy and Astrophysics.* Vol 614. 2018 June.

Reiners, A. et al. (2018a) "The CARMENES search for exoplanets around M dwarfs. HD147379 b: A nearby Neptune in the temperate zone of an early-M dwarf" in *Astronomy and Astrophysics.* Letters to the Editor. L5. 2018 January.

Reiners, A. et al. (2018b) "The CARMENES search for exoplanets arund M dwarfs. High-resolution optical and near-infrared spectroscopy of 324 survey stars" in *Astronomy and Astrophysics.* Vol 612, A49. 2018 April.

Ribas, I. et al. (2018) "A candidate super-Earth planet orbiting near the snow line of Barnard's star" in *Nature.* Vol 563, pp. 365-368. 2018 November.

Ricker, G.R. et al. (2015) "Transiting Exoplanet Survey Satellite (TESS)" in *Journal of Astronomical Telescopes, Instruments, and Systems.* Vol. 1. 2015 January

Safronov, V.S. (1972) "Evolution of the protoplanetary cloud and formation of the earth and planets". Israel Program for Scientific Translations, Keter Publishing House. 1972.

Schneider, J. et al. (2011) "Defining and cataloguing exoplanets: the exoplanet.eu database" in *Astronomy and Astrophysics.* Vol.532. 2011.

Soter, S. (2006) "What is a planet?" in *The Astronomical Journal.* Vol 132, pp. 2513–2519. 2006.

Spiegel, D. et al. (2020) "The Deuterium-Burning Mass Limit for Brown Dwarfs and Giant Planets" in *The Astrophysical Journal.* Vol. 727 number 1. 2011 January.

Stevens, D.J. and Gaudi, B.S (2013) "A posteriori transit probabilities" in *Publications of the Astronomical Society of the Pacific.* Vol.125, pp. 933–950. 2013 August.

Stock, S. et al. (2020) "The CARMENES search for exoplanets around M dwarfs. Characterization of the nearby ultra-compact multiplanetary system YZ Ceti" in Astronomy and Astrophysics. Vol 636. 2020.

Strang, G. (1986) "Introduction to Applied Mathematics" Wellesley-Cambridge Press. 758pp (p.398). ISBN 0-9614088-0-4. 1986.

Suarez Mascareno, A. et al. (2017) "HADES RV Programme with HARPS-N at TNG. V.- A super-Earth on the inner edge of the habitable zone of the nearby M dwarf GJ 625" in *Astronomy and Astrophysics.* Vol 605. 2017 September.

Suarez-Mascareno, A. et al. (2017) "A super-Earth orbiting the nearby M dwarf GJ 536" *in Astronomy and Astrophysics.* Vol 597. 2017 January.

Sumi, T. et al. (2010) "A Cold Neptune-Mass Planet OGLE-2007-BLG-368Lb: Cold Neptunes Are Common" in *The Astrophysical Journal.* Vol. 710, number 2. 2010 February.

Trifonov, T. et al. (2018) "The CARMENES search for exoplanets around M dwarfs. First visual-channel radial-velocity measurements and orbital parameter updates of seven M-dwarf planetary systems" in *Astronomy and Astrophysics.* Vol 609. 2018.

Tuomi, M. et al. (2014) "Bayesian search for low-mass planets around nearby M dwarfs – Estimates for occurrence rate based on global detectability statistics" in *Monthly Notices of the Royal Astronomical Society.* pp. 1 – 31. 2014 March.

Tuomi, M. et al. (2018) "AD Leonis: Radial Velocity Signal of Stellar Rotation or Spin–Orbit Resonance?" in *The Astronomical Journal.* Vol 155, pp. 192-209. 2018 May.

William D.C. et al. (1991) "Constraints on The Companion Object to HD114762" in *The Astrophysical Journal.* Vol. 380, L35-L38. 1991 October

Wolszczan, A. and Frail, D. A. (1992). "A planetary system around the millisecond pulsar PSR1257 + 12" in *Nature.* Vol. 355, pp. 145–147. 1992

Wright, D.J. et al. (2016) "Three Planets Orbiting Wolf 1061" in *The Astrophysical Journal Letters.* Vol. 817, letter 20. 2016 February.

Zechmeister, M. et al. (2019) "The CARMENES search for exoplanets around M dwarfs. Two temperate Earth-mass planet candidates around Teegarden's Star" in *Astronomy and Astrophysics.* Vol 627. 2019.

ANNEX I.- INDIVIDUAL ANALYSIS OF "STAR 1"

The objective of describing this individual analysis for a single star is to facilitate the understanding of the method applied to derive de detection limits for the sample of stars in the CARMENES survey. Left panel in Figure AI.1 shows the radial velocity time series for Star 1. A first inspection by eye is enough to look for peculiarities that would need a particular analysis (trends with time, anomalies, etc.). Otherwise, we proceed with the calculation of the periodogram, showed in right panel of AI.1, along with the window function of the radial velocity time series.
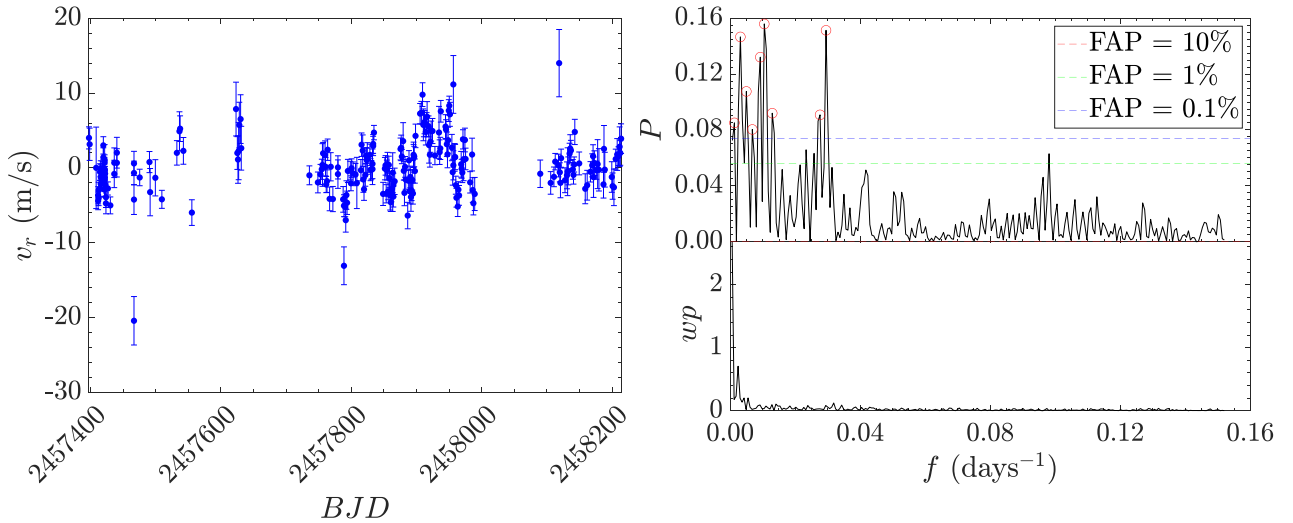

Figure AI. 1.- Left: Observed radial velocities for the Star 1, spanning ~800 days. Right: Periodogram (top panel) and window function (bottom panel) computed for the radial velocity time series. Dashed lines indicate the 10%, 1% and 0.1% FAP threshold with different colours as labelled. A total of 9 frequencies are significant above the 0.1% FAP probability threshold commonly considered in exoplanet studies.

Signals below FAP = 0.1% (above the FAP corresponding frequency power) are associated with real stellar or planetary signals, which are fully investigated and modelled if a planet is detected. Therefore, to estimate the underlying level of noise in the data, needed to compute the planet detection limit in this data, we fit a model including $v_{model} = A + \sum_{i=1}^{9}[B_i \sin(2\pi f_i t) + C_i \cos(2\pi f_i t)]$. The result of this fit is shown in Figure AI.2 as well as the residuals after the fitting. Next, we study which is the minimum signal we are able to detect at this noise level, the detection limit.

As explained in section 3, to estimate the detection limit, we produce 1000 permutations of the residuals and calculate the corresponding periodograms. By doing this we obtain 1000 power values compatible with no planet for each period tested. Next, we introduce a sinusoidal mock signal for each frequency to be tested and we increase its

amplitude until we are able to detect it. We consider that the signal is detectable when, after calculating the periodogram, the obtained frequency power is higher than 99% of the noise compatible powers. By doing this for each frequency we obtain a vector of radial-velocity semi-amplitudes that we can transform to minimum masses using equation 5 in section 3.3. Figure AI.3 illustrates the minimum mass as a function of the period.
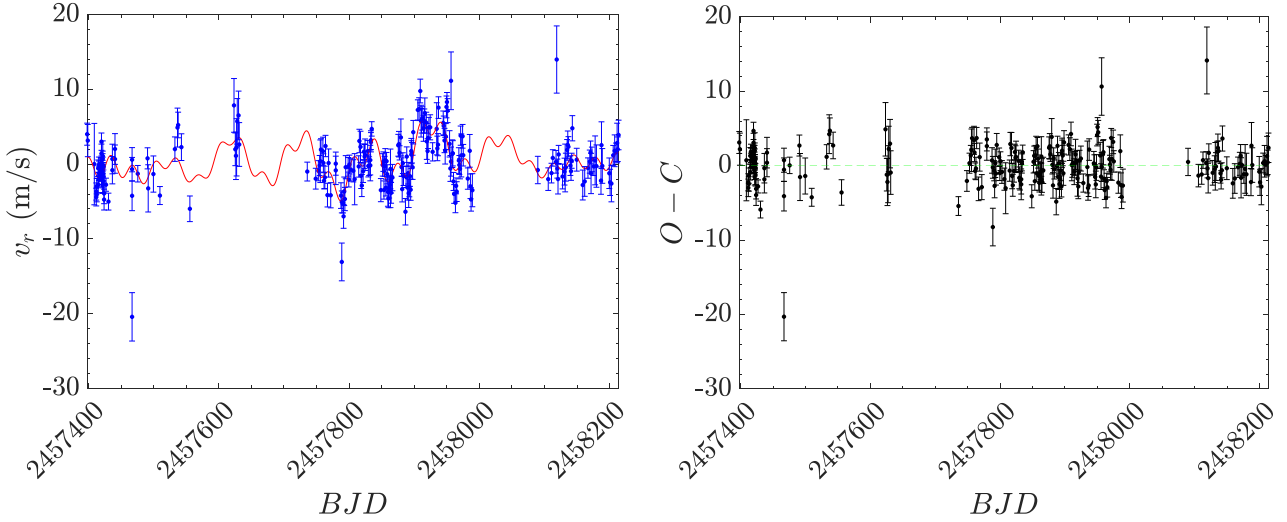

Figure AI. 2.- (Left) Obtained model obtained to fir Star 1 time series and (Right) residuals after subtracting the signal.

In this diagram we observe that in the residuals of "Star 1" after eliminating the periodical components, any planet above $6M_\oplus$ (super-Earth) with a period shorter than 100 days would have been detected. This result is only an example of the employed method to derive the detection limits.
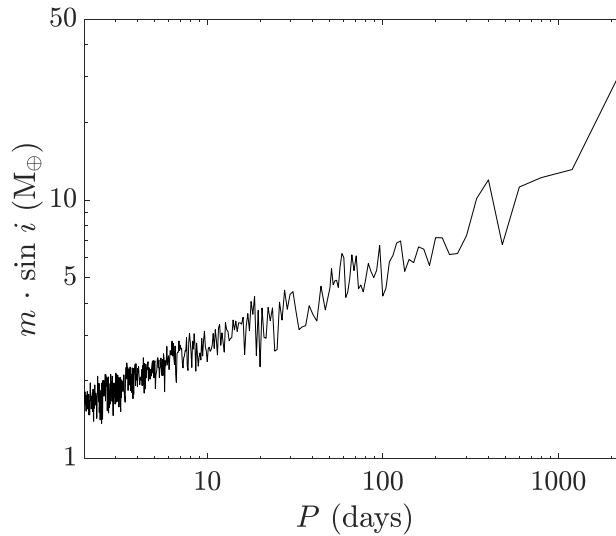

Figure AI. 3.- Planet detection limit for Star 1. This P vs $m{\cdot}\sin i$ diagram represents the minimum planet mass that can be detected considering the residuals of Star 1 radial velocities after removing all periodic detectable signals.

ANNEX II.- NOISE COMPUTATION FOR STARS WHICH PRESENT LONG PERIOD VARIABILITY

Several stars in the sample show radial velocity trend with respect time which could be due to periodic signals with long periods that have not been still fully sampled. This is the case of stars number 69, 285, 291, and 304. They show some periodic modulation with longer periods than those used by the periodogram to calculate the powers of the frequencies, longer than the Nyquist frequency. We can see this in several ways: representing the time series, from the periodogram or from the calculation of the residuals. Using visual inspection is often enough to observe the trend and proceed to manual adjustment. If we look at the periodograms of these signals, we see that, often, the first frequency tested has a value above the FAP. In most of the cases it is not enough to fit a signal to the data with this frequency since its value is not necessarily correct. As it is the first frequency tested, it actually indicates an upper limit of the real frequency.

Another way to infer the presence of a long period signal is from the analysis of the residuals obtained by fitting to the peak frequencies of the period. If the data does not fit correctly, finding a background noise comparable to the observations, we should think that we are not properly removing some of the signals present. The objective of this annex is to explain the individual analysis done for these four stars, as well as to give the values of the estimated periods.

Left panel in Figure AII.1 shows the observed radial velocities for star number 69. It shows a clear decreasing trend that indicates a long-period modulation. In the right panel of Figure AII.1 the periodogram is drawn with the window function of the radial velocity time series. Two signals below 0.01 days^{-1} exceed the 0.1% FAP threshold, being the most powerful of them indeterminate, but below the first frequency sampled. Only adjusting to the well-determined frequency, we do not obtain a consistent fit so we must consider longer period than the ones tested. In the left panel of Figure AII.2 the best fitting is plotted from which we obtain a frequency $f = (1.59 \pm 1.9) \cdot 10^{-4}$ days^{-1}, given with 95% confidence interval (Figure AII.2.-Left). In the right panel the periodogram computed after removing this signal from data is shown. We see how the lowest frequency peaks have disappeared, and yet two new frequencies appear. From this moment we apply the procedures used for the rest of the stars. From the same fitting we obtained a semi-amplitude of 59.9 km/s, which combined

with the obtained period of ~ 6290 days give an estimated mass of the stelar companion ~ 1075 $M_\oplus$. However, this is only a result obtained with the objective of calculating the residuals and we would need a greater number of observations for a correct analysis.
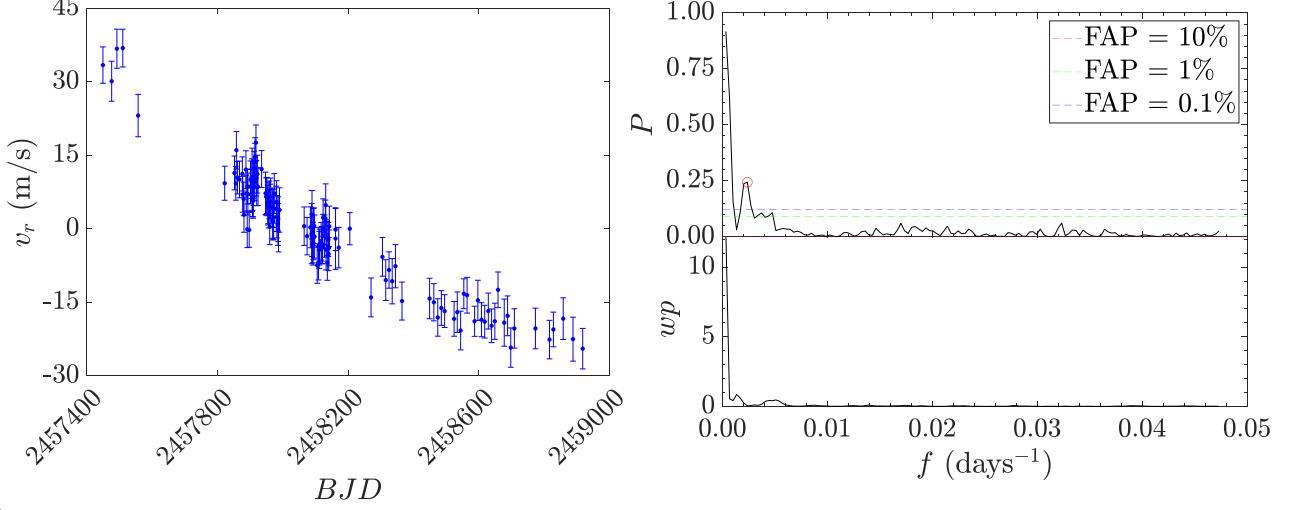

Figure AII. 1.- Left: Radial velocity data observed for Star 69. A long period modulation is appreciated. Right: Periodogram (top panel) and window function (bottom panel) of the radial velocity timeseries for star 69. As can be seen the first frequency tested far exceeds the 0.1% FAP which is an indicator of a long period signal.
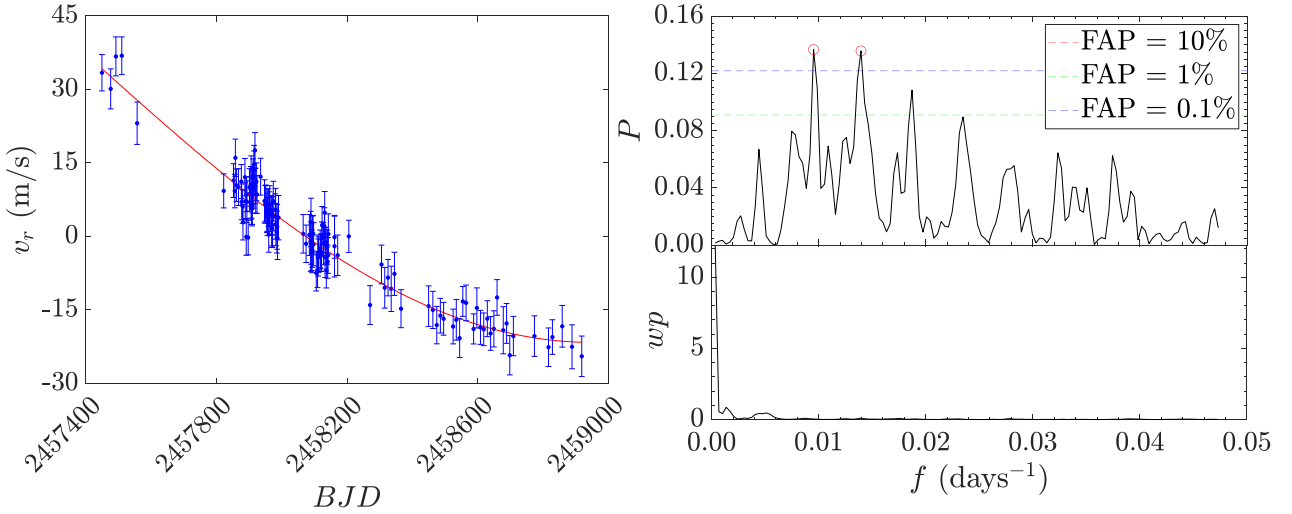

Figure AII. 2.- Left: Radial velocity data observed for Star 69 fitted to a sinusoidal equation of frequency $f = (1.59 \pm 1.9) \cdot 10^{-4}$ days^{-1}. Right: Periodogram (top panel) and window function (bottom panel) of the radial velocity time series for star 69 after removing the long period signal. Two new peaks with higher frequencies appear.

The fitted radial velocity series for stars 285 and 304 are shown in Figure AII.3. From the best fittings we obtain periods of 2513 and 730 days, respectively. These signals could be associated with stellar companions of 2440 and 18000 $M_\oplus$. These values, although only

preliminary estimates, can be used to devise the best strategy to plan future observations in order to resolve the origin of the signals. Star 285 corresponds to GJ849, so the variability is due to a long period known planet orbiting around it. On the other hand, the variability observed for star 304 is probably due to stellar activity since a great activity it is a known active star.
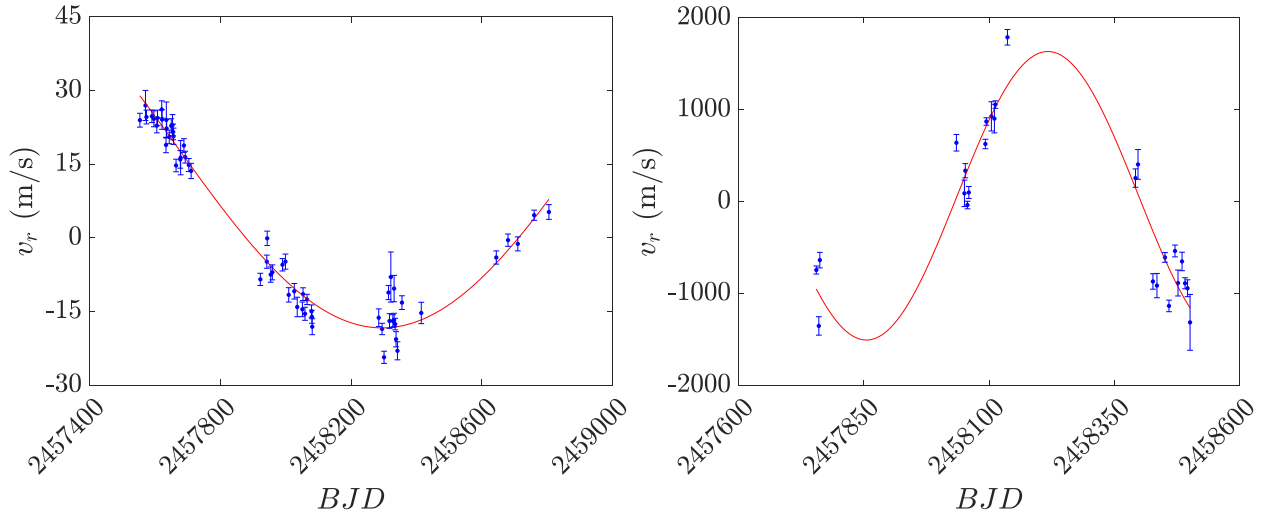

Figure AII. 3.- Left: sinusoidal fit to radial velocity data for star 285. Right: sinusoidal fit to radial velocity data for star 304.

The case of star 291 is especially particular. In the top-left panel of Figure AII.4 we cannot see any long period sinusoidal signal but an ascending linear trend throughout the observation period. In the top-right panel, when computing the associated periodogram, a peak is resolved at frequencies close to zero and the first frequency exceeds the FAP $= 0.1\%$. In this case we decided to fit the data to a line of slope $m = 0.002482$ m/s·days^{-1}. In the bottom left panel the fitted line can be found. In bottom-right panel we can see that, as a result of this fitting, the computed periodogram does not exhibit the first peaks. when computing again the periodogram. It probably corresponds to an annual alias for the long period.
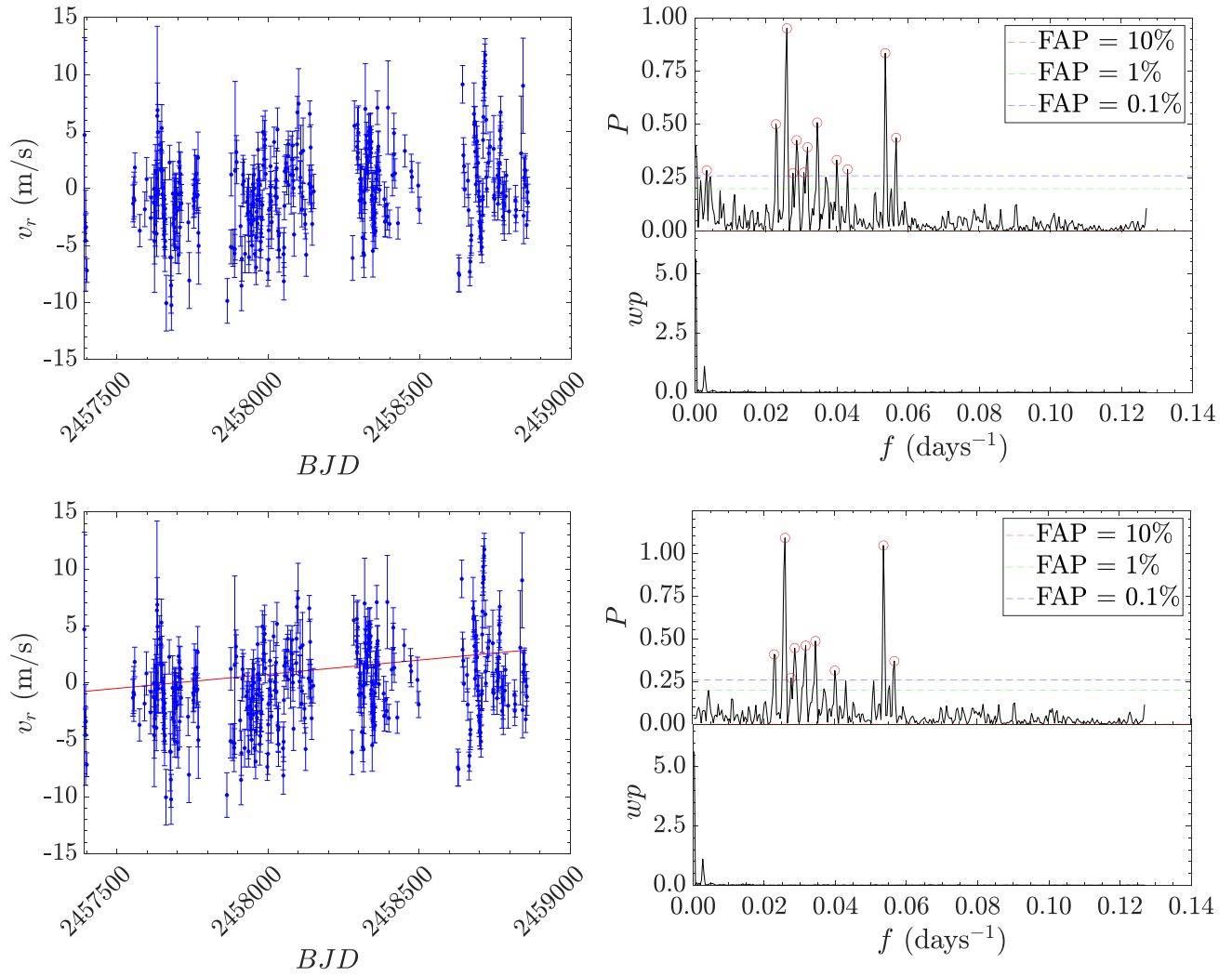
Figure AII. 4.- Top-left panel: radial velocity data observed for Star 291. An ascending linear trend is observed. Top-right panel: periodogram (top panel) and window function (bottom panel) of the radial velocity timeseries for star 291 showing two low-frequency peaks above the 0.1% FAP power threshold. Bottom-left panel: linear fit and data observed for star 291. Bottom-right panel: periodogram (top panel) and window function (bottom panel) of the residuals of star 291 after subtracting the linear trend. It can be seen that both low-frequency peaks disappear.